Modeling the Interaction between Cumulus Convection and Linear Gravity Waves Using a Limited-Domain Cloud System–Resolving Model

ZHIMING KUANG

Department of Earth and Planetary Sciences, and School of Engineering and Applied Sciences, Harvard University, Cambridge, Massachusetts

(Manuscript received 10 January 2007, in final form 14 June 2007)

ABSTRACT

A limited-domain cloud system–resolving model (CSRM) is used to simulate the interaction between cumulus convection and two-dimensional linear gravity waves, a single horizontal wavenumber at a time. With a single horizontal wavenumber, soundings obtained from horizontal averages of the CSRM domain allow the large-scale wave equation to be evolved, and thereby its interaction with cumulus convection is modeled. It is shown that convectively coupled waves with phase speeds of 8–13 m s^{-1} can develop spontaneously in such simulations. The wave development is weaker at long wavelengths ($>\sim$10 000 km). Waves at short wavelengths ($\sim$2000 km) also appear weaker, but the evidence is less clear because of stronger influences from random perturbations. The simulated wave structures are found to change systematically with horizontal wavelength, and at horizontal wavelengths of 2000–3000 km they exhibit many of the basic features of the observed 2-day waves. The simulated convectively coupled waves develop without feedback from radiative processes, surface fluxes, or wave radiation into the stratosphere, but vanish when moisture advection by the large-scale waves is disabled. A similar degree of vertical tilt is found in the simulated convective heating at all wavelengths considered, consistent with observational results. Implications of these results to conceptual models of convectively coupled waves are discussed. In addition to being a useful tool for studying wave–convection interaction, the present approach also represents a useful framework for testing the ability of coarse-resolution CSRMs and single-column models in simulating convectively coupled waves.

1. Introduction

How cumulus convection interacts with large-scale circulations is a long-standing problem in meteorology and remains poorly understood. One class of such an interaction, namely, that of convectively coupled waves, has attracted much attention (e.g., Lindzen 1974; Emanuel 1987; Neelin et al. 1987; Wang 1988; Takayabu 1994; Wheeler and Kiladis 1999; Mapes 2000; Majda and Shefter 2001; Sobel and Bretherton 2003; Haertel and Kiladis 2004, hereafter HK04; Fuchs and Raymond 2005; Khouider and Majda 2006). In addition to being quite well observed, their apparent linear characteristics suggest that they may serve as a good starting point for more general investigations of the interaction between cumulus convection and the large-scale circulation.

Various numerical experiments using cloud system–resolving models (CSRM) have been used to simulate these waves (e.g., Grabowski and Moncrieff 2001; Kuang et al. 2005; Tomita et al. 2005; Tulich et al. 2007). In these studies, large domain sizes (thousands of kilometers or more) are used to accommodate the large-scale waves. In this paper, we model this interaction in a limited-domain CSRM. Inspired by the observed linear characteristics of these waves, we study each individual horizontal wavenumber separately. This methodology is explained in more detail in section 2. Section 3 contains a description of the model that we use and the experimental setup. The simulation results are described in section 4. Additional implications to conceptual models of convectively coupled waves are discussed in section 5, followed by the conclusions in section 6.

Corresponding author address: Zhiming Kuang, Department of Earth and Planetary Sciences, and School of Engineering and Applied Sciences, Harvard University, 20 Oxford St., Cambridge, MA 02138.
E-mail: kuang@fas.harvard.edu

DOI: 10.1175/2007JAS2399.1

2. Methodology

Let us start by considering the two-dimensional (2D) anelastic linearized perturbation equations of momentum, continuity, and hydrostatic balance. In the following, all equations are for the large-scale wave:

$$\bar{\rho}u'_t = -p'_x - \varepsilon\bar{\rho}u', \tag{1}$$

$$(\bar{\rho}u')_x + (\bar{\rho}w')_z = 0, \tag{2}$$

$$p'_z = \bar{\rho}g\frac{T'}{\overline{T}}, \tag{3}$$

where ε is the mechanical damping coefficient and all other symbols assume their standard meteorological meaning. The background mean variables are denoted with an overbar. We treat a single horizontal wavenumber k at a time, and thus assume solutions of the form

$$[u', w', T', p'](x, z, t) = \text{real}\{[\hat{u}, \hat{w}, \hat{T}, \hat{p}](z, t)\exp(-ikx)\}. \tag{4}$$

The lower boundary condition is $w' = 0$ and the radiation upper boundary condition is (see, e.g., Durran 1999, his section 8.3.2)

$$\hat{p} = \bar{\rho}\hat{w}N/|k|, \tag{5}$$

where N is the buoyancy frequency at the upper boundary and $N^2 = (g/\overline{T})[(d\overline{T}/dz) + (g/c_p)]$.

Eliminating u' and p' from Eqs. (1)–(3) and applying Eq. (4), we have

$$\left[\left(\frac{\partial}{\partial t} + \varepsilon\right)(\bar{\rho}\hat{w})_z\right]_z = -k^2\frac{\bar{\rho}g}{\overline{T}}\hat{T}. \tag{6}$$

For a given $x = x_0$, for which we multiply Eq. (6) by $\exp(-ikx_0)$ and take the real component, we have

$$\left\{\left(\frac{\partial}{\partial t} + \varepsilon\right)[\bar{\rho}w'(x_0, z, t)]_z\right\}_z = -k^2\frac{\bar{\rho}g}{\overline{T}}T'(x_0, z, t). \tag{7}$$

We now use the CSRM domain to represent the atmospheric column at $x = x_0$. When only a single horizontal wavenumber is present, T' along this vertical line, computed as the deviation of the CSRM domain-averaged temperature profile from a reference profile,[1] can be used with both Eq. (7) and the boundary conditions to evolve w' of the large-scale wave along this vertical line. Effects of this vertical velocity are then included in the CSRM integration as source terms of temperature and moisture, applied uniformly in the horizontal. Integration of the CSRM produces new domain-averaged profiles of temperature and moisture, the equations of which may be written as

$$T'_t + w'\left(\frac{d\overline{T}}{dz} + \frac{g}{c_p}\right) = S'_T, \tag{8}$$

$$q'_t + w'\frac{d\overline{q}}{dz} = S'_q, \tag{9}$$

where all variables are at $x = x_0$, and S'_T and S'_q are the perturbation temperature and moisture tendencies resulting from cumulus convection simulated explicitly by the CSRM. The new (virtual) temperature profile is then used again in Eq. (7) to update w' for the next time step, completing the interaction between wave and convection. Because the sign of the wavenumber does not enter in the calculation, the results can be viewed as representing a vertical line in either eastward- or westward-propagating waves or in standing waves (excluding the nodal points).

The present approach may be viewed as the cloud-resolving cumulus parameterization (CRCP) approach (Grabowski 2001), with the large-scale dynamics reduced to that of a single linear wave. It is also similar in spirit to recent suggestions for using a limited-domain CSRM or a single-column model with parameterized large-scale dynamics to study the sensitivity of convection to various forcings (Sobel and Bretherton 2000; Bergman and Sardeshmukh 2004; Mapes 2004; Raymond and Zeng 2005). Indeed, Eq. (6) is the same as $\partial/\partial z$ of Eq. (A3) of Bergman and Sardeshmukh, and the treatment of vertical advection in Eqs. (8) and (9) is standard. The previous studies, however, were not formulated to model convectively coupled waves. While using a limited-domain CSRM, as opposed to a large-domain CSRM, does allow substantial savings in computation, the more important advantage of the present approach is the simplicity brought about by the simplified large-scale dynamics (linear waves of a single horizontal wavenumber). We do leave out aspects of the convection–wave coupling, such as the nonlinear interactions between waves of different scales, but these aspects may be better addressed in future studies after the simpler problem of interaction between convection and linear waves is better understood.

3. Model and experimental setup

We have implemented the above procedure in the System for Atmospheric Modeling (SAM) version 6.4, which is a new version of the Colorado State University Large Eddy Simulation/Cloud Resolving Model [see Khairoutdinov and Randall (2003) for details about the model]. Briefly, the model uses the anelastic equations

[1] In the actual integration, virtual temperature is used.

of motion, and the prognostic thermodynamic variables are the liquid water static energy, total nonprecipitating water, and total precipitating water. The model uses bulk microphysics with the following five types of hydrometeors: cloud water, cloud ice, rain, snow, and graupel. For this study, we use a simple Smagorinsky-type scheme for the effect of subgrid-scale turbulence, and for simplicity we compute the surface fluxes using the bulk aerodynamic formula with constant exchange coefficients and surface wind speed. The surface temperature is set to 29.5°C.

To be more representative of the conditions over convective regions in the tropics, we prescribe the background vertical velocity profile (shown in Fig. 1) to be that averaged over the large-scale array (LSA) during the intensive operating period (IOP) of the Tropical Ocean Global Atmosphere Coupled Ocean–Atmosphere Response Experiment (TOGA COARE; Webster and Lukas 1992) from 1 November 1992 through 28 February 1993, using the gridded product by Ciesielski et al. (2003). Background vertical shear is not included in this study.

For each of our simulations, we first run the model as a conventional CSRM, that is, without coupling to gravity wave dynamics, for 30 days (referred to as the background integration). Coupling is then activated and the model is integrated for another 70 days. Unless otherwise noted, a 10-day mechanical damping time scale is used. This value is more appropriate for the free troposphere but is applied uniformly at all heights for simplicity. The radiative tendency profile is prescribed and constant in time throughout the simulations. This profile and the initial temperature and moisture profiles are the statistical equilibrium profiles from an earlier long integration of the model as a conventional (uncoupled) CSRM with interactive radiation. The radiation schemes used are those of the National Center for Atmospheric Research (NCAR) Community Climate Model (CCM3; Kiehl et al. 1998). For simplicity, we have removed the diurnal cycle as in our previous studies (Kuang and Bretherton 2004).

We have verified that in the background integration, after the first few days, there is little drift in temperature and moisture over all heights in the troposphere, and we use averages over the last 10 days to define the background temperature and moisture profiles, and thus the background virtual temperature profile. This is used as the reference profile for computing the perturbation (virtual) temperature in Eq. (3) after coupling to gravity wave dynamics is activated. After this coupling is activated, for simplicity, the background vertical velocity acts only on the background vertical temperature and moisture profiles and represents a constant forcing of the CSRM.

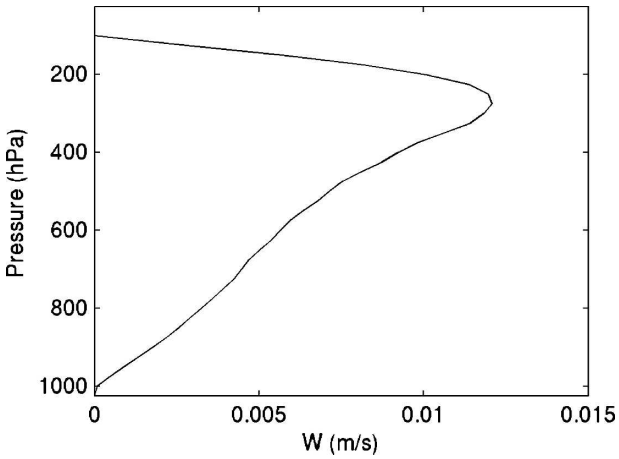

FIG. 1. Prescribed large-scale vertical velocity in the simulations.

The horizontal resolution is 2 km and there are 64 points in the vertical, with the vertical grid size varying from 75 m near the surface to 500 m in the middle and upper troposphere and to about 1 km near the domain top (at 32 km). A wave-absorbing layer is placed over the upper third of the domain. Note that this layer only affects waves explicitly simulated by the CSRM. The upper boundary condition for the large-scale wave is Eq. (5). Unless otherwise noted, the domain has 192 × 192 grid points in the horizontal. The SAM integration uses a variable time step determined by its Courant–Friedrichs–Lewy (CFL) number, and the integration of the large-scale gravity wave equation uses a time step of 1 min. The domain averages are sampled every time step and output every 3 h. Because of the finite domain size of the CSRM, viewing it as a vertical line in the large-scale wave field is an idealization and assumes that the horizontal scale of the wave is much larger than the CSRM domain size. Thus, we shall only apply this method to waves with wavelengths of thousands of kilometers or more.

4. Results

Figure 2 shows the time series of the domain-averaged precipitation of a set of experiments with horizontal wavenumbers [units of $2\pi(1000\ \text{km})^{-1}$] of 0.5, 0.35, 0.2, 0.15, 0.1, 0.075, and 0.05 (or wavelengths of 2000, 2857, 5000, 6667, 10 000, 13 333, and 20 000 km). Before coupling to wave dynamics is activated, the CSRM produces a domain-averaged precipitation with a mean value of 9.1 mm day^{-1} and a standard deviation of 0.6 mm day^{-1}. After coupling is activated, pro-

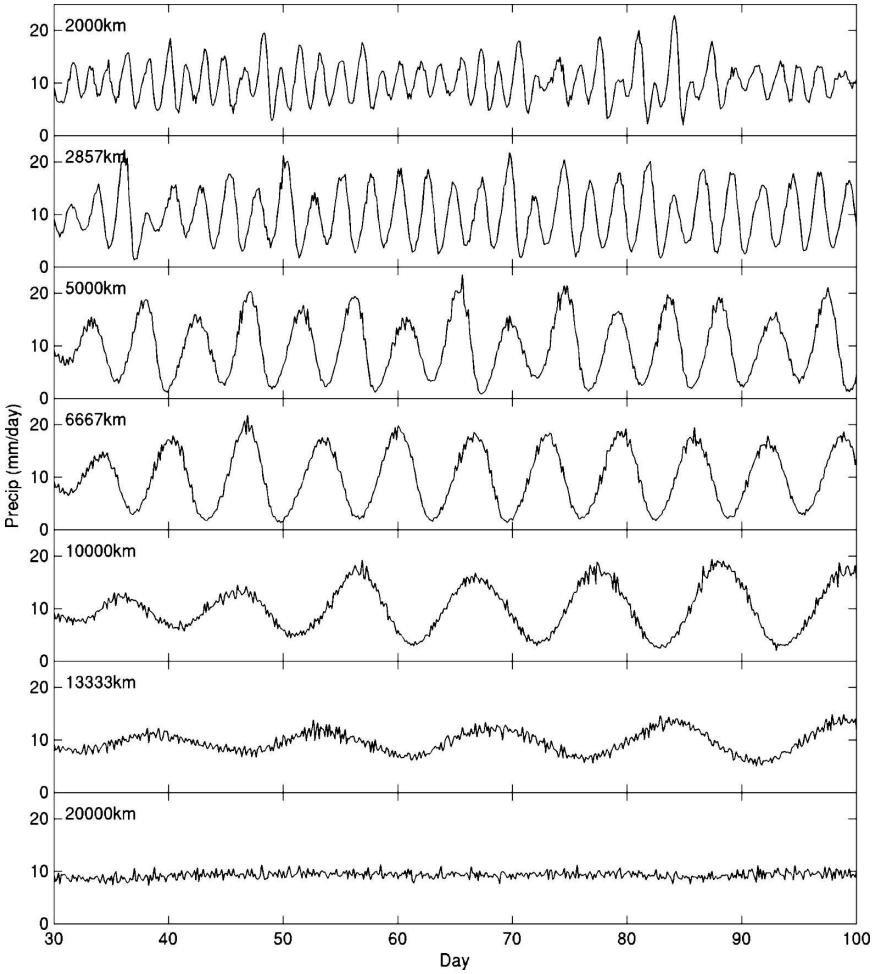

FIG. 2. Domain-averaged precipitation as a function of time after coupling to gravity wave is activated for wavelengths of (top to bottom) 2000, 2857, 5000, 6667, 10 000, 13 333, and 20 000 km.

nounced oscillations develop spontaneously in all cases except at 20 000 km. As the wavelength increases beyond 10 000 km, it takes longer for the oscillation to grow to its equilibrated amplitude and the equilibrated amplitude also decreases. Since the 13 333 km case does not appear to have reached its equilibrated amplitude in Fig. 2, we have run it for another 50 days and its amplitude remains unchanged from that over the last 20 days shown in Fig. 2.

There is also a tendency for the wave amplitude to decrease as wavelength decreases beyond 5000 km. This is not as clear because oscillations at shorter wavelengths are less regular, owing to random perturbations by convection on the domain-averaged virtual temperature profiles. At shorter wavelengths, virtual temperature perturbations of a given size produce larger vertical velocity perturbations [Eq. (6)]. This makes the shorter-wavelength cases more susceptible to the effect of these random perturbations so the simulations are not as clean. The random virtual temperature perturbations are smaller with a larger domain. The horizontal domain size of 192×192 points was chosen largely as a balance between this consideration and the computational cost. With smaller domains, the oscillation becomes stronger and more irregular at short wavelengths (Figs. 3a,b), although at wavelengths of 5000 km and longer, effects from such random perturbations are small, and the results are not sensitive to domain size (Figs. 3c,d).

Amplitudes achieved by the mid-/long-wavelength waves are affected by the mechanical damping time scale. Representative results with a mechanical damping time of 4 days and with no mechanical damping are shown in Figs. 4 and 5, respectively. Stronger damping reduces the amplitude that medium-/long-wavelength waves, particularly the long-wavelength waves, can

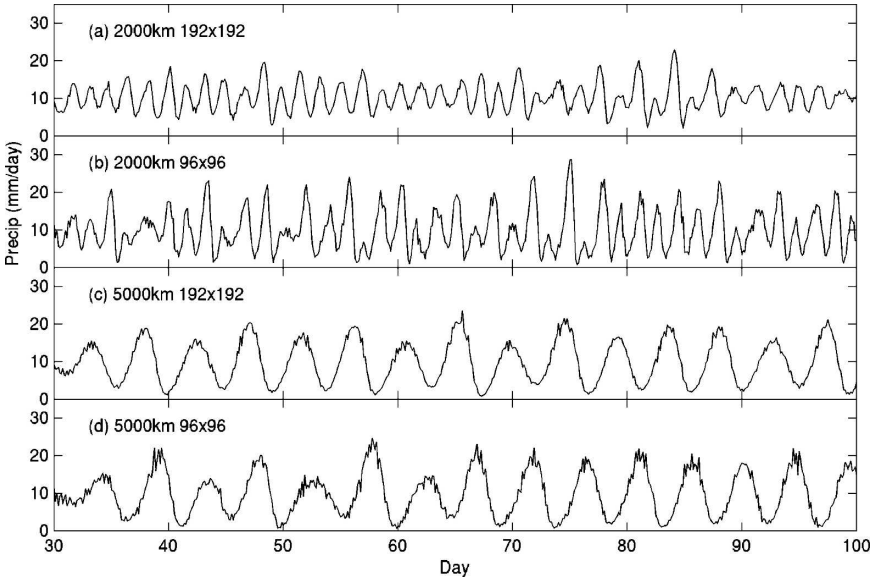

FIG. 3. Domain-averaged precipitation as a function of time for wavelengths of (a), (b) 2000 and (c), (d) 5000 km. A horizontal domain of 192 × 192 grid points is used in (a) and (c), and a horizontal domain of 96 × 96 grid points is used in (b) and (d).

achieve. With no mechanical damping or sufficiently weak damping and strong wave growth, the waves equilibrate at amplitudes approximately equal to that of the basic-state convection (20 000 km, the no-damping case eventually reaches this amplitude as well), and the positive (stronger precipitation) phase can achieve greater amplitude (in terms of departure from the background mean) than the negative (weaker

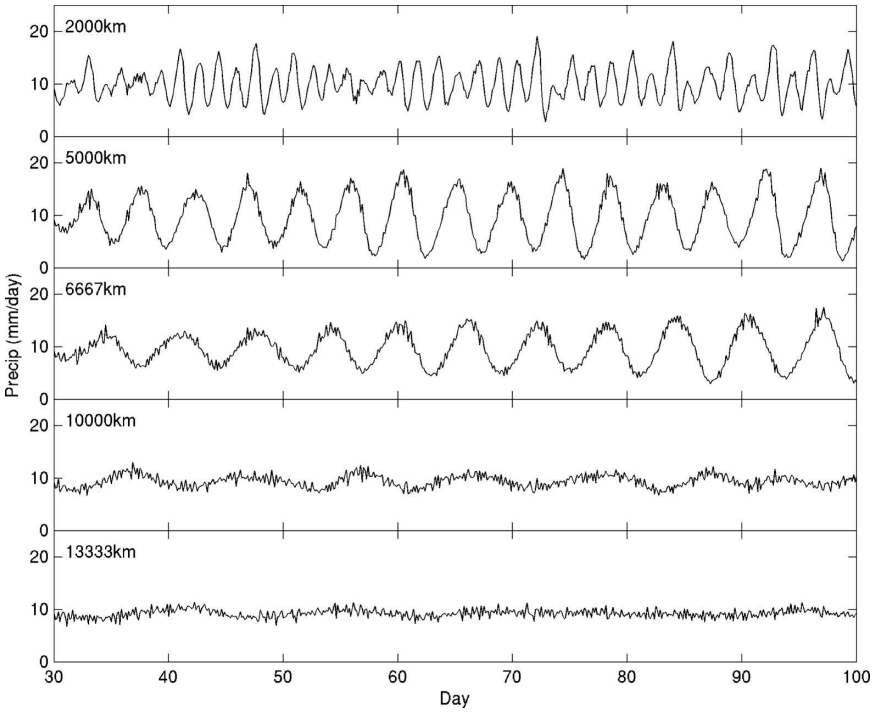

FIG. 4. Same as Fig. 2, but for representative cases with a mechanical damping time of 4 days.

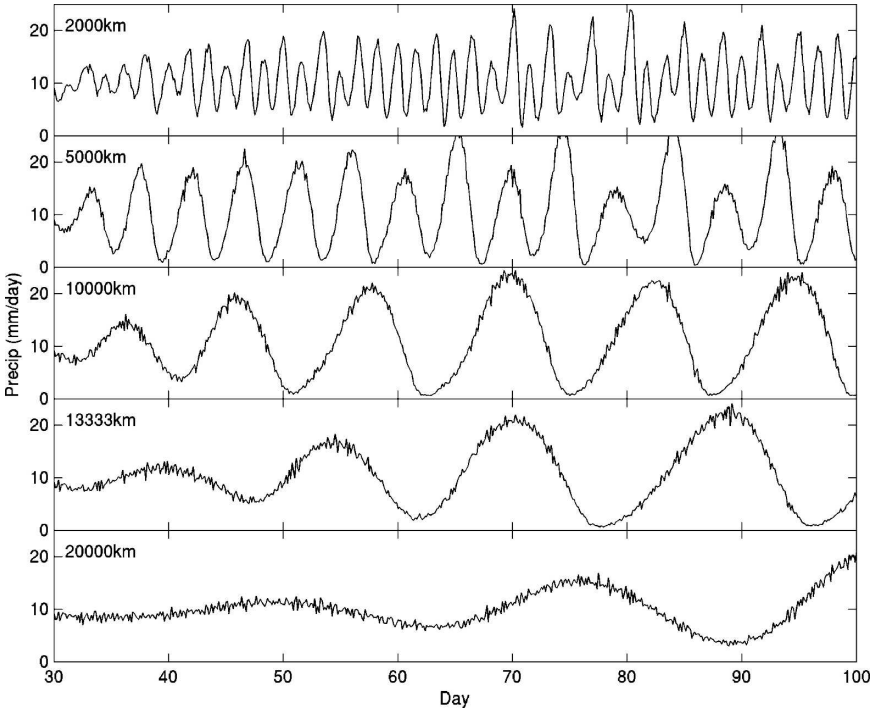

FIG. 5. Same as Fig. 2, but for representative cases with no mechanical damping.

precipitation) phase. The bound on the negative phase is presumably due to the fact that precipitation cannot be negative. The bound on the positive phase must also result from nonlinearity intrinsic to convection because the large-scale waves here are strictly linear. We defer the discussion of nonlinearity to a later study, but note that while it cannot address the full nonlinear interaction between wave and convection because of the assumption of linear wave dynamics, the present methodology can still be a useful simplifying framework for studying nonlinearity intrinsic to convection and its role in wave–convection coupling.

For all damping values, the wave growth at long wavelengths is slower. This is true in simulations without mechanical damping as well, even though in this case the equilibrated wave amplitudes at long wavelengths are as large as those at medium wavelengths (Fig. 5). Figure 6 attempts to quantify this. We first do a running mean of the precipitation time series to remove the subdaily variations. We then identify the local maxima that occur after coupling to wave dynamics is activated, and use linear interpolation to compute the wave amplitude for the positive phase at each time. The wave amplitude is taken to be 0 at the time when coupling to wave dynamics is activated. The solid line in Fig. 6 shows the time for the wave amplitude of the positive phase to grow to 3 mm day^{-1} (an arbitrary choice, but using other values does not change the conclusion). Repeating the calculation using the minima gives the dashed line in Fig. 6. These estimates are less reliable for the shorter wavelengths, so only the results for the longer wavelengths are shown. There is a clear tendency for smaller growth rates at longer wavelengths beyond a few thousand kilometers. It is worth noting that a simple conceptual model of convectively

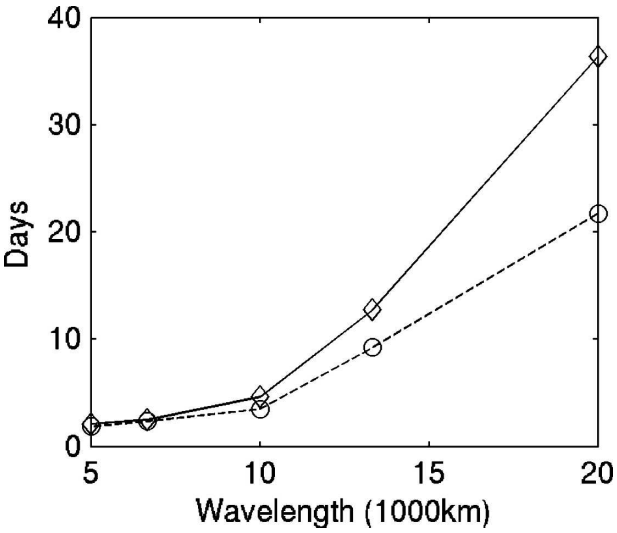

FIG. 6. Time for the wave amplitude of the positive (dashed, circle) and negative (solid, diamond) phases to grow to 3 mm day^{-1} in the no-mechanical-damping cases.

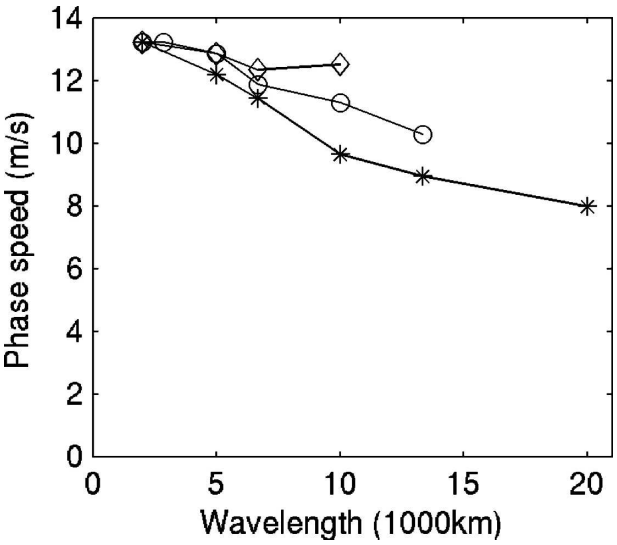

FIG. 7. Estimated wave phase speeds at different wavelengths with a mechanical damping time of 4 (diamonds) and 10 days (circles), and with no mechanical damping (asterisks).

coupled waves constructed and analyzed by Kuang (2008) produces this behavior of smaller growth rates at longer wavelengths, and part of the reason for this behavior in that model is the damping effect due to convection's tendency to remove moisture anomalies.

Figure 7 shows the phase speeds of the simulated waves. The period is estimated as twice the lag time for which the autocorrelation of precipitation is most negative. Other ways, such as dividing the elapsed time by the number of cycles in between, produce similar results. There is a tendency for the phase speeds to be slower at longer wavelengths and with weaker damping. Closer examination indicates that the wave periods tend to be longer when the waves are saturated (i.e., with amplitudes roughly equal to that of the basic-state convection). How wavelength and nonlinearity intrinsic to convection might affect the wave speeds could be a topic worthy of further investigation.

Figure 8–10 show the structures of the simulated oscillations at wavelengths of 2000, 5000, and 10 000 km, along with estimated phase speeds. The structures are constructed by regressing various fields onto precipitation anomalies with a range of lags. For a given wavelength, all fields are scaled by a factor so that the minimum in the composite precipitation is -10 mm day^{-1}. This is done to facilitate a comparison across the different wavelengths. We only show the results with a 10-day mechanical damping time; the results for the 4-day-damping and no-damping cases are similar. Figure 8 may be compared with the structure of 2-day waves (HK04, their Fig. 4), because the two have simi-

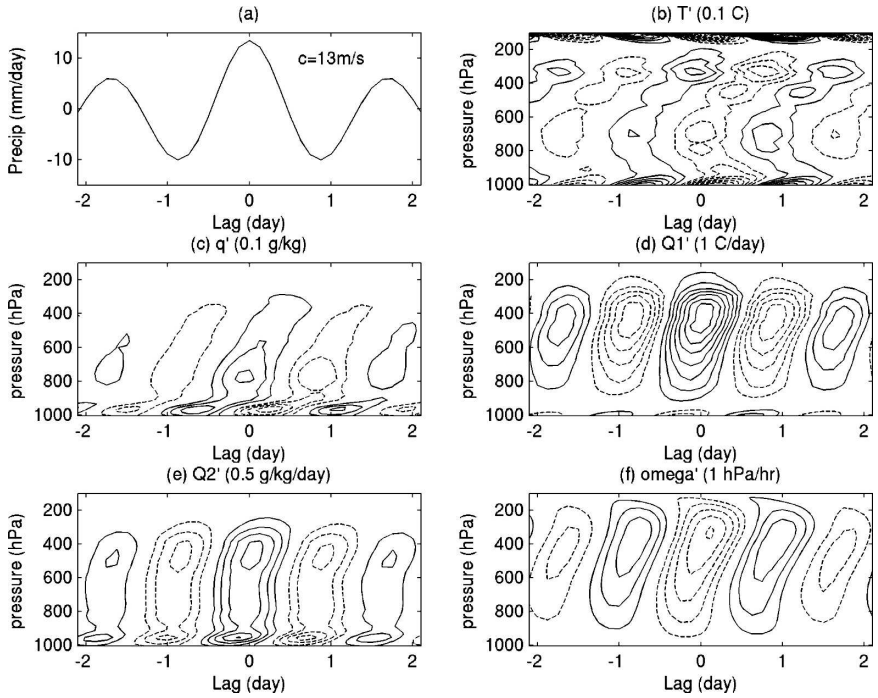

FIG. 8. Composite wave structures for the wavelength of 2000 km: (a) precipitation, (b) temperature, (c) specific humidity, (d) convective heating, (e) convective drying, and (f) vertical pressure velocity. Contour intervals are indicated above each plot. Negative contours are dashed and the zero contours are omitted. The estimated phase speed is shown in (a).

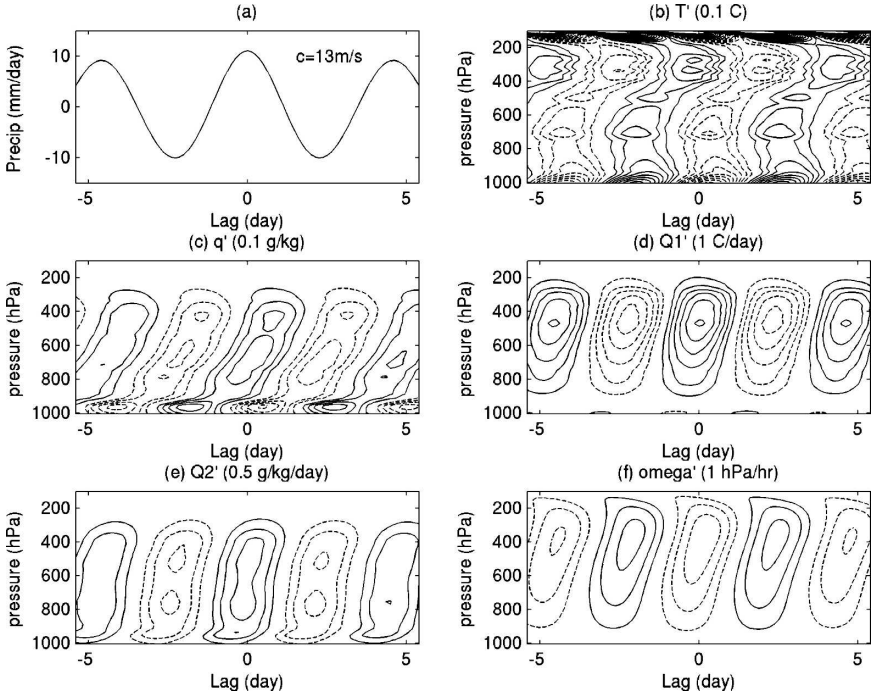

FIG. 9. Same as Fig. 8, but for the wavelength of 5000 km.

lar wave periods. The comparison shows a good resemblance in their basic features. This includes the following: the near-surface temperature is roughly in phase (out of phase) with the lower-tropospheric (upper tropospheric) temperature; cold anomalies tend to coincide with dry anomalies for the near-surface air, while the opposite relationship exist in the lower troposphere between ~600 and ~900 hPa; convective heating above

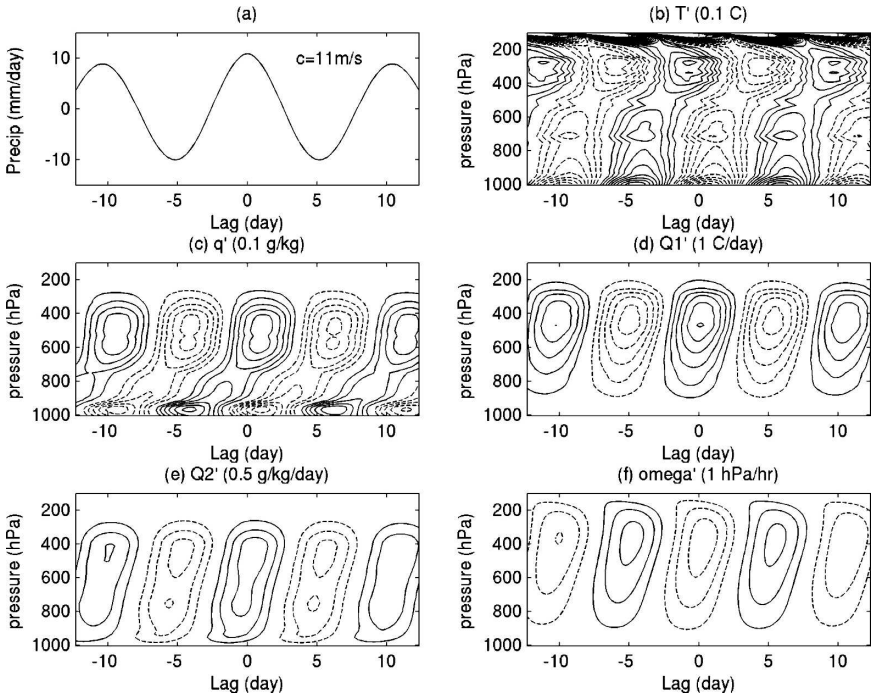

FIG. 10. Same as Fig. 8, but for the wavelength of 10 000 km.

the subcloud layer (the cloud base is located at ~930 hPa, or 670 m) has a tilted structure, with the anomalies progressing from the lower to the upper troposphere; and at times of enhanced (reduced) convective heating in the lower troposphere, there is enhanced (reduced) convective cooling and drying in the subcloud layer. While the resemblance is quite good, there are some differences as well. For example, the simulated temperature/moisture anomalies above the subcloud layer are somewhat smaller than those observed for 2-day waves, while those in the subcloud layer are larger (the convective heating anomalies are of similar magnitude). Also, peaks of the temperature anomalies in the lower troposphere are between 750 and 800 hPa for the observed 2-day waves, while those in the simulation are located somewhat higher at around 700 hPa. Many factors may contribute to such differences. First of all, our experiments are for 2D gravity waves. The 2-day waves defined in HK04 differ from 2D gravity waves in some potentially important ways: they are affected by planetary rotation and propagate westward only, and their meridional scale of convection is narrower than that of their dynamical fields (see, e.g., Fig. 3 of HK04). Also, while we prescribe the mean vertical velocity based on TOGA COARE, we do not include mean horizontal advection or use nudging to match the mean thermodynamic profiles to the observed ones. Furthermore, while the resolution employed here is typical of today's CSRM simulations, they are too coarse to simulate shallow convection accurately (and are far from achieving numerical convergence). Aspects of the model, for example, the microphysics, also may not be sufficiently accurate. It is not yet clear which factors are responsible for the differences between the results in Fig. 8 and those of the 2-day waves. While ultimately one would like the numerical models to simulate all aspects of the observed waves well, this is beyond the scope of the present study. The goal here is to capture the basic features in a simple setting. By this measure the simulated waves are sufficiently similar to the observed ones to lend us confidence that results here will be relevant to convectively coupled waves in the real atmosphere, notwithstanding the aforementioned caveats. We have tested the effect of various simplifications (used mostly for ease of interpretation) in our experimental design. For instance, when the CSRM is coupled to gravity wave dynamics, we have the background vertical velocity act on the background temperature and moisture profiles so that it represents a constant forcing on the CSRM. In the real atmosphere, the background vertical velocity would instead act on the actual vertical temperature and moisture profiles. We have also assumed a uniform mechanical damping time scale for simplicity, while in reality we expect stronger damping in the lower troposphere. We have performed simulations with the background vertical velocity advecting the actual vertical temperature and moisture profiles, and with the damping time scale decreasing linearly from 10 days at 5 km (and above) to 1 day at 1 km (and below). Such changes affect the details of simulated wave patterns, but not their basic features.

One may also compare the 5000-km case (Fig. 9) with the observed Kelvin wave structure (Fig. 5 of Straub and Kiladis 2003). The comparison is not as clear-cut as in the 2-day- and 2000-km-wave case, where both waves have similar coherence, estimated here by how fast the envelope amplitude of the composite precipitation decreases with increasing lag (Fig. 2b of HK04; Fig. 8a herein). The coherence of the observed Kelvin waves, seen from Fig. 5a of Straub and Kiladis (2003), with outgoing longwave radiation in place of precipitation, is substantially lower than that of the simulated 5000-km waves shown in Fig. 9a. This indicates that the observed Kelvin wave structures may include contributions from a range of wavelengths. Notwithstanding the above differences, the most basic patterns in the two figures are still in reasonable agreement.

Comparing Figs. 8–10 reveals systematic changes in the wave structure with wavelength. This is true at the other wavelengths as well (Fig. 11). While the q' patterns have a backward-tilted structure in all cases, the anomaly in the midtroposphere (between 400 and 600 hPa) increases substantially with wavelength relative to those in the lower troposphere (between 700 and 900 hPa). There is also a tendency for temperature anomalies in the lower troposphere to become more in phase with the subcloud-layer moist static energy as the wavelength increases. Some indications of these changes can be seen in observations as well. Comparing the observed structures of Kelvin waves (Fig. 5 in Straub and Kiladis 2003) and 2-day waves (Fig. 4 in HK04), the Kelvin waves have longer wavelengths and their temperature anomalies in the lower troposphere are more in phase with the subcloud-layer moist static energy. Their moisture anomalies between 700 and 900 hPa are also not as prominent as those of the 2-day waves. These changes may be related to the difference between the wave period and the internal convective time scales, and are interesting features that need to be explained by theories of wave–convection interaction. Amplitudes of the moisture and temperature anomalies also increase with wavelength, especially at longer wavelengths where the increase is about linear. This is expected because we have normalized the waves based on precipitation, which is roughly proportional to vertical velocity. Temperature/moisture variations per unit

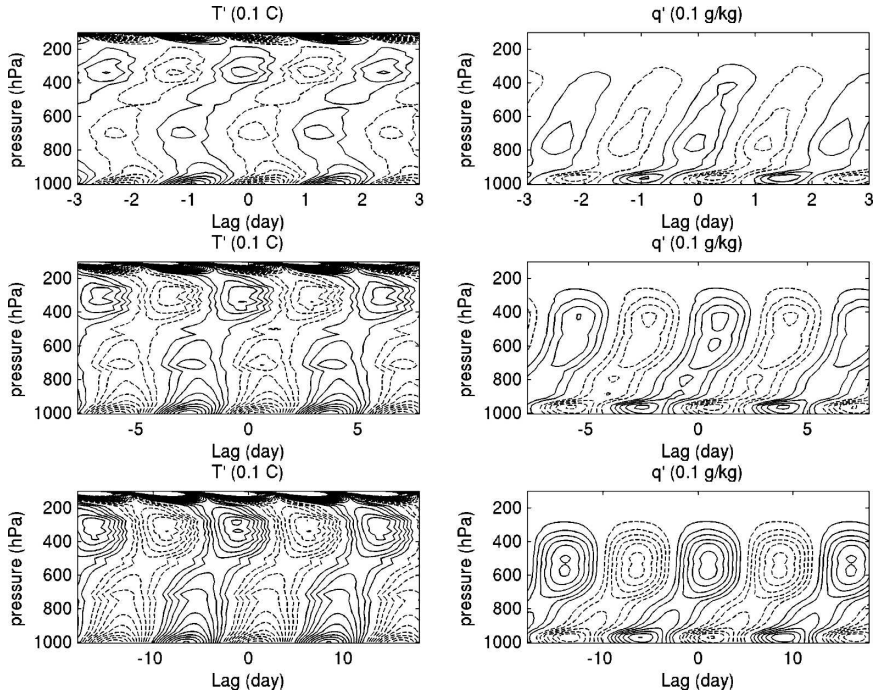

FIG. 11. Same as Fig. 8, but for (left) temperature and (right) specific humidity at wavelengths of (top) 2857, (middle) 6667, and (bottom) 13 333 km.

vertical velocity variation tend to increase with wavelength (or wave period), as seen in Eqs. (8) and (9).

In a study of the 2-day waves, HK04 showed that the first two vertical modes based on a vertical mode decomposition, assuming a rigid lid at 150 hPa, can capture the basic features of the heating and temperature patterns. We have done a similar vertical decomposition with a rigid lid at 14 km. In the literature, the method of Fulton and Schubert (1985) is typically used to solve for eigenmodes of the vertical structure equation

$$\Omega_{zz} + \frac{k^2}{c_j^2} N^2 \Omega = 0,$$

where Ω is the vertical structure function for $\bar{\rho}w$ and c_j are the phase speeds of the free vertical modes. We have used the Matlab solver for eigenproblems and found it to be adequate. Figures 12 and 13 show the results for the wavelength of 5000 km. Results for other wavelengths are similar. The first two vertical modes (with dry speeds of 49 and 23 m s^{-1}, respectively) capture the heating structure very well and the residues are small. The first two modes also capture the general patterns of the temperature anomalies in the bulk of the troposphere, but not the details; temperature anomalies of higher vertical modes are present. These results are similar to the findings of HK04 for the 2-day waves. While replacing the radiation upper boundary condition by a rigid lid is an approximation, simulations with a rigid lid at 14 km (to be described in section 5a), for which the vertical mode decomposition is exact,

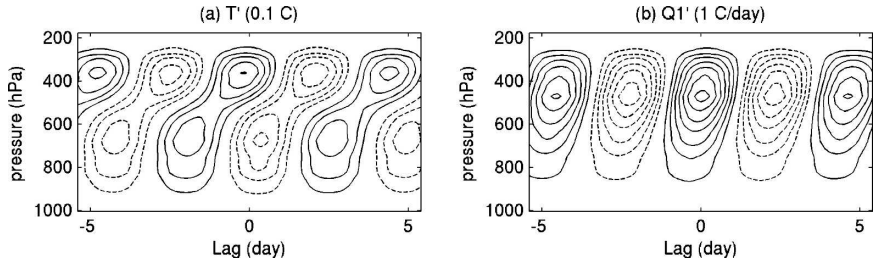

FIG. 12. (a) Temperature and (b) convective heating structures reconstructed from the first two vertical modes.

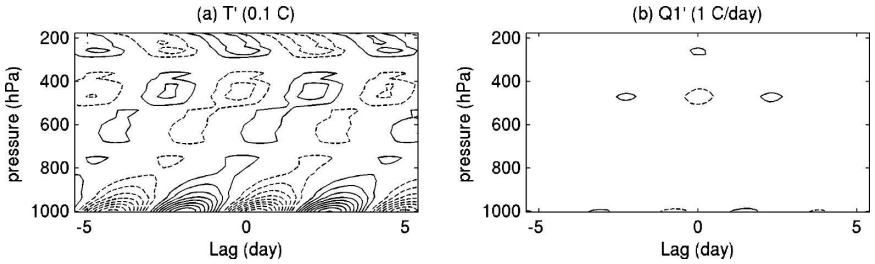

FIG. 13. Residues in (a) temperature and (b) convective heating from reconstructing with the first two vertical modes.

give similar results. A major feature not captured by the first two vertical modes is temperature anomalies in and near the subcloud layer, which are distinct from anomalies above and peak near the surface. Moisture anomalies in and near the subcloud layer are also distinct from those above, and tend to peak just below the cloud base (located near 930 hPa). These results support the notion (although by no means guarantee) that a model that consists of the first two vertical modes and the subcloud layer might be able to represent the basic dynamics of convectively coupled waves.

5. Discussions

a. Instability mechanisms

A number of mechanisms have been suggested as being important for generating convectively coupled waves and in setting their phase speeds, such as the wind-induced surface heat exchange (WISHE) mechanism (Emanuel 1987; Neelin et al. 1987), wave radiation into the stratosphere (Lindzen 1974; Lindzen 2003), stratiform instability (Mapes 2000), and moisture feedback (Khouider and Majda 2006). The WISHE mechanism is absent in our simulations because we use a bulk aerodynamic formula with a constant wind speed; so are feedbacks from radiation because radiative tendencies are prescribed and constant in time. To evaluate the importance of wave radiation into the stratosphere, we replace the radiation upper boundary condition [Eq. (5)] by a rigid-lid condition ($w' = 0$) at 14 km. In this case, the development of convectively coupled waves (Fig. 14) and the basic wave patterns remain the same (Fig. 15 shows the results for the wavelength of 5000 km; other wavelengths are similar). The main change is that with a rigid lid, large-scale waves no longer propagate into the stratosphere. Temperature anomalies near the very top of Fig. 15 are above the rigid lid and solely are due to the convective heating there. In this simulation, we have also held the surface fluxes constant in time (at appropriate values) to completely eliminate feedbacks from surface fluxes (either positive or negative). This has no effect on our conclusion about the role of wave radiation into the stratosphere, but reinforces the conclusion that surface flux feedbacks are not essential for the simulated waves.

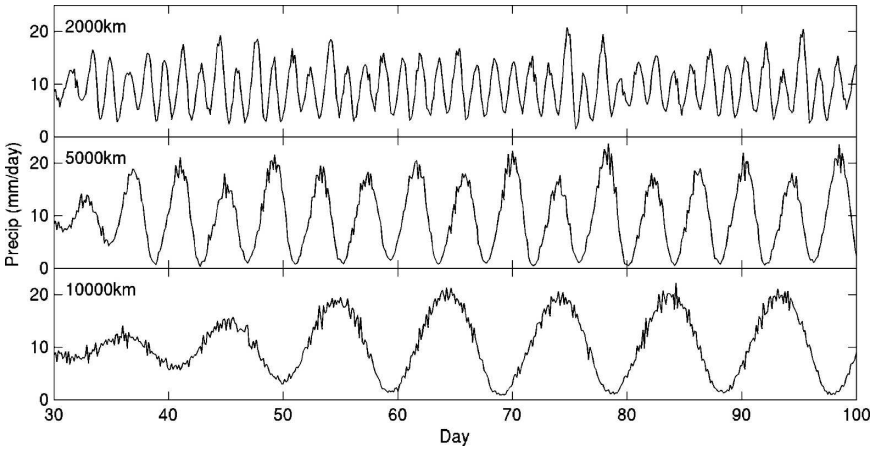

FIG. 14. Same as Fig. 2, but when a rigid-lid condition is used at 14 km and for wavelengths of 2000, 5000, and 10 000 km.

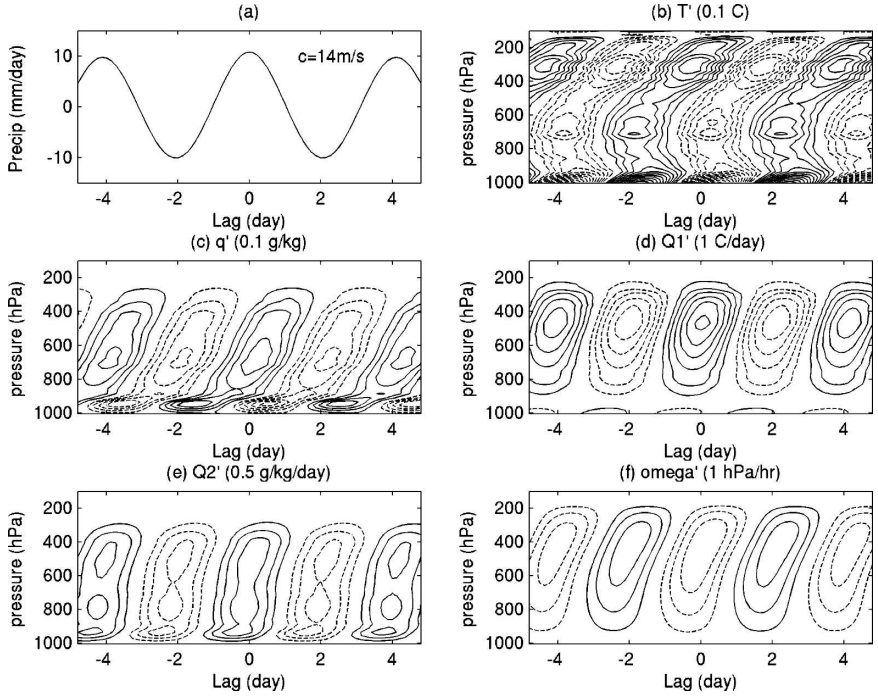

FIG. 15. Same as Fig. 9, but with a rigid lid at 14 km and constant surface heat fluxes.

We now remove vertical moisture advection by the large-scale waves by having wave vertical velocity acting only on temperature but not on moisture. This eliminates the convectively coupled waves as shown in Fig. 16 for wavelengths of 2000, 5000, and 10 000 km. The remaining variations in precipitation are presumably due to random variations in convection. This demonstrates that vertical advection of moisture by large-scale waves is essential to the existence of convectively coupled waves. The effect of moisture on convection must also be essential because convection is the way by which moisture can in turn affect the large-scale waves. While moisture also directly affects density, and hence the waves, through the virtual effect, this effect is small and secondary, as confirmed by experiments in which the virtual effect is neglected when integrating the large-scale wave equations. The importance of moisture–convection feedback was previously shown in the context of Madden–Julian oscillation–like coherences (Grabowski and Moncrieff 2004). Their simulations

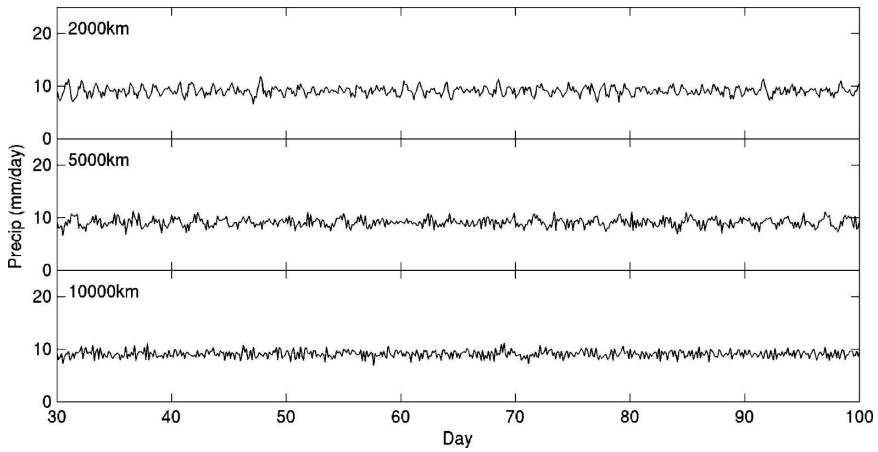

FIG. 16. Same as Fig. 2, but with vertical advection of moisture by large-scale waves disabled and for wavelengths of 2000, 5000, and 10 000 km.

were done on a global domain using the CRCP approach, and moisture variations were suppressed by nudging. The demonstration here is arguably cleaner because it avoids nudging. The essentialness of moisture effect demonstrated here is in contrast to the view expressed in Mapes' original simple tropical wave model (Mapes 2000), which neglects the moisture effect. In more recent developments, free-tropospheric moisture is included as an important component (Khouider and Majda 2006; Kuang 2008), and an instability that arises from feedback between wave, convection, and free tropospheric moisture is illustrated in Fig. 11 of Kuang (2008).

b. *Parameterization of stratiform heating in models with two vertical modes*

Many current stratiform instability models (Mapes 2000; Majda and Shefter 2001; Khouider and Majda 2006) parameterize stratiform heating through a lagged relationship to deep convective heating (typically with a fixed time lag of 3 h). This follows the treatment of Mapes (2000) and is based on the life cycle of mesoscale convective systems (MCS). However, a fixed time lag implies that as wavelength increases, the phase lag between deep convective and stratiform heating (measured in radians), and hence the tilt in the heating structure, will become increasingly small. This is not consistent with the present simulations, where a similar degree of tilt in the heating structure is seen at all wavelengths (Figs. 8–11). To quantify this, we shall take the first vertical mode (from the vertical decomposition described in section 4) as the deep convective heating, and the second mode as the congestus (when it is positive) and stratiform heating (when negative). In other words, we are viewing the CSRM simulations in a two vertical model framework. Following earlier studies (e.g., Mapes 2000; Khouider and Majda 2006), the word "stratiform" ("congestus") is used in this context to refer to a heating anomaly structure that is positive (negative) aloft and negative (positive) below, with the view that such a heating anomaly is associated with enhanced (reduced) stratiform and/or reduced (enhanced) congestus cloud populations, similar to that depicted in Fig. 11 of Mapes et al. (2006). We then compute the lagged correlation between the strength of two heating modes, and the lag between deep convective and stratiform heating is defined as the lag with the most negative correlation. The results are shown in Fig. 17 for the various wavelengths. It is clear that when the CSRM simulations are interpreted in a two vertical mode framework, stratiform heating does not lag convective heating by a fixed time. A better approximation

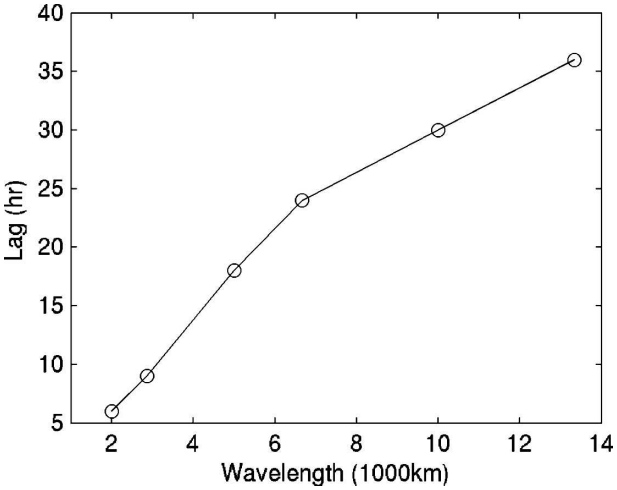

FIG. 17. The estimated lag between deep convective heating and stratiform heating as a function of wavelength.

instead is the lag increasing roughly linearly with wavelength (or wave period). The results remain the same for simulations with a rigid lid, in which case the vertical mode decomposition is exact. Similar conclusions were reached in observational studies (Kiladis et al. 2005; Mapes et al. 2006). Therefore, in large-scale convectively coupled waves, stratiform heating cannot be tied to deep convective heating with a fixed lag, as in MCSs (and many of the current stratiform instability models). Other factors must be modulating the strength of stratiform heating. Midtropospheric humidity appears a likely candidate. That midtropospheric humidity can affect tropical deep convection is well supported by observations, numerical simulations, and theoretical reasoning (Brown and Zhang 1997; Sherwood 1999; Parsons et al. 2000; Redelsperger et al. 2002; Ridout 2002; Derbyshire et al. 2004; Takemi et al. 2004; Roca et al. 2005; Kuang and Bretherton 2006). With all else being equal, a dry midtroposphere is unfavorable to deep convection because lateral entrainment of drier environmental air by the rising air parcels leads to more evaporative cooling, and hence negative buoyancy. We hypothesize that from the perspective of large-scale wave–cumulus interaction, the midtropospheric humidity is the main control on the depth of convection: when the midtroposphere is moist, cumulus ensembles can reach higher, and thus have a larger stratiform heating component; when the midtroposphere is dry, cumulus ensembles are limited to lower altitudes, and thus have a larger congestus heating component. This is consistent with the results shown in Figs. 8–11, and appears to be an attractive way for determining stratiform/congestus heating in conceptual models.

c. *Quasi equilibrium*

An important way to conceptualize the interaction between large-scale circulation and cumulus convection is the concept of quasi equilibrium (QE; Arakawa and Schubert 1974), which states that convection should maintain a state of statistical equilibrium with the large-scale flow. In some previous simple models of wave–convection interaction (Emanuel et al. 1994), the approximate invariance of convective available potential energy (CAPE) is used as a simplification for QE over the whole depth of the troposphere. Such models of wave–convection interaction do not yield instability without WISHE or other destabilization mechanisms, and therefore do not explain the development of convectively coupled waves in our simulations. The model by Mapes (2000) does not utilize the QE concept, and instead emphasizes triggering and inhibition. We agree that triggering and inhibition are important aspects of cumulus dynamics, however, they reflect more of a view on individual storm scale; and on the large scale, conceptual simplification may still be achieved through a quasi-equilibrium view. The composite wave structures in Figs. 8–11 suggest a plausible simplification of QE. They show that temperature in the lower troposphere [instead of the entire free troposphere, as in Emanuel et al. (1994)] is more or less in phase with the boundary layer moist static energy, especially at long wavelengths. This is seen in the observational study by Sobel et al. (2004) as well. It therefore appears that near invariance of a shallow CAPE, defined as the integrated buoyancy for undiluted parcels only up to the midtroposphere, may be a more suitable simplification to QE than the deep CAPE traditionally used. The problem with using the near invariance of the deep CAPE is that the effect of lateral entrainment is neglected. As discussed in the previous subsection, lateral entrainment is a very important aspect that makes the height of convection sensitive to tropospheric moisture. By using a shallow CAPE, we by no means imply that cloud parcels do not experience entrainment in the lower troposphere. However, the cumulative effect of entrainment is smaller in the lower troposphere because of the shorter distance traveled by the cloud parcels and their smaller moist static energy difference from the environment. Therefore, it may be a reasonable simplification to neglect the effect of lateral entrainment over the lower half of the troposphere, and only include it further up through the control of midtropospheric humidity on the depth of convection. These ideas will be discussed in more detail in Kuang (2008), who describes a simple model of the convectively coupled waves.

6. Concluding remarks

In this paper, we demonstrate that a limited-domain CSRM coupled with linear wave dynamics can be used to simulate wave–cumulus interaction. With this approach, convection is simulated in three dimensions at a relatively high resolution without overwhelmingly high computational cost, and the large-scale dynamics is simplified to that of linear gravity wave of a single horizontal wavenumber. This reduces the problem to a very simple setting for studying wave–cumulus interaction.

Convectively coupled waves with phase speeds of 8–13 m s^{-1} can develop spontaneously in these simulations. The wave development is weaker at long wavelengths ($>\sim$10 000 km). Waves at short wavelengths ($\sim$2000 km) also appear weaker, although the evidence is less clear because the short wavelengths are more susceptible to the effect of random perturbations from the CSRM simulations. The simulated wave structures at horizontal wavelengths of 2000–3000 km resemble those of the observed 2-day waves in their basic features. The simulated wave structures are found to change systematically with the horizontal wavelength, an interesting behavior that needs an explanation from theories of wave–cumulus interaction. The separate integration of large-scale dynamics and the CSRM (in the same way as in the CRCP approach) enables us, for example, to turn off moisture advection by the large-scale waves and replace the upper boundary condition for the large-scale waves in a straightforward manner. Our results indicate that convectively coupled waves can develop without feedbacks from radiative processes, surface fluxes, or wave radiation into the stratosphere, but vanish when moisture advection by the large-scale waves is disabled. The tilt in the convective heating pattern is found to remain roughly the same at all wavelengths considered. This challenges the treatment in many current models (Mapes 2000; Majda and Shefter 2001; Khouider and Majda 2006), where stratiform heating is treated as lagging deep convective heating by a fixed time lag, and indicates that other factors must be controlling the strength of stratiform heating. We suggest midtropospheric humidity as a likely candidate. The simulations also show that, similar to observations, temperature in the lower troposphere is roughly in phase with the boundary layer moist static energy. This suggests that some simplified treatment of QE might be used to gain conceptual simplification of the wave–convection interaction. A conceptually simple model of convectively coupled waves has been constructed based on these considerations (Kuang

2008). The simulation results here have been further used to constrain the parameters of that model.

While the present approach includes only one horizontal wavenumber a time, it includes all vertical wavenumbers and is suitable for studying how the observed vertical structures are selected. We have focused on results for one background mean state, namely, that with the mean vertical velocity of TOGA COARE, but have experimented with other background mean states (e.g., without the mean vertical velocity or with additional horizontal moisture advection). In these cases, convectively coupled waves can also develop spontaneously, but the strength of the instability varies substantially with the background mean states. Documenting and understanding how the waves and the instability change with the mean state is a problem of considerable interest and is currently being investigated. Because of its simplicity, the present approach is also a useful framework for testing the performance of single-column models with parameterized cumulus dynamics and coarse-resolution CSRMs in simulating convectively coupled waves. Results from such tests will be reported in future publications.

Acknowledgments. The author thanks Marat Khairoutdinov for making the SAM model available; Dave Raymond, Adam Sobel, Stefan Tulich, and an anonymous reviewer for their constructive reviews; and Chris Walker for helpful comments. The author also wishes to acknowledge Dr. Scott Fulton's generosity for making his vertical transform code available, even though the code was not eventually used in this paper. This work was supported partly by the Modeling, Analysis and Prediction (MAP) Program in the NASA Earth Science Division.

REFERENCES

Arakawa, A., and W. H. Schubert, 1974: Interaction of a cumulus cloud ensemble with the large-scale environment, Part I. *J. Atmos. Sci.,* **31,** 674–701.

Bergman, J. W., and P. D. Sardeshmukh, 2004: Dynamic stabilization of atmospheric single column models. *J. Climate,* **17,** 1004–1021.

Brown, R. G., and C. D. Zhang, 1997: Variability of midtropospheric moisture and its effect on cloud-top height distribution during TOGA COARE. *J. Atmos. Sci.,* **54,** 2760–2774.

Ciesielski, P. E., R. H. Johnson, P. T. Haertel, and J. H. Wang, 2003: Corrected TOGA COARE sounding humidity data: Impact on diagnosed properties of convection and climate over the warm pool. *J. Climate,* **16,** 2370–2384.

Derbyshire, S. H., I. Beau, P. Bechtold, J.-Y. Grandpeix, J.-M. Piriou, J.-L. Redelsperger, and P. M. M. Soares, 2004: Sensitivity of moist convection to environmental humidity. *Quart. J. Roy. Meteor. Soc.,* **130,** 3055–3079.

Durran, D. R., 1999: *Numerical Methods for Wave Equations in Geophysical Fluid Dynamics.* Springer-Verlag, 465 pp.

Emanuel, K. A., 1987: An air–sea interaction model of intraseasonal oscillations in the Tropics. *J. Atmos. Sci.,* **44,** 2324–2340.

——, J. D. Neelin, and C. S. Bretherton, 1994: On large-scale circulations in convecting atmospheres. *Quart. J. Roy. Meteor. Soc.,* **120,** 1111–1143.

Fuchs, Z., and D. J. Raymond, 2005: Large-scale modes in a rotating atmosphere with radiative–convective instability and WISHE. *J. Atmos. Sci.,* **62,** 4084–4094.

Fulton, S. R., and W. H. Schubert, 1985: Vertical normal mode transforms: Theory and application. *Mon. Wea. Rev.,* **113,** 647–658.

Grabowski, W. W., 2001: Coupling cloud processes with the large-scale dynamics using the Cloud-Resolving Convection Parameterization (CRCP). *J. Atmos. Sci.,* **58,** 978–997.

——, and M. W. Moncrieff, 2001: Large-scale organization of tropical convection in two-dimensional explicit numerical simulations. *Quart. J. Roy. Meteor. Soc.,* **127,** 445–468.

——, and ——, 2004: Moisture-convection feedback in the tropics. *Quart. J. Roy. Meteor. Soc.,* **130,** 3081–3104.

Haertel, P. T., and G. N. Kiladis, 2004: Dynamics of 2-day equatorial waves. *J. Atmos. Sci.,* **61,** 2707–2721.

Khairoutdinov, M. F., and D. A. Randall, 2003: Cloud resolving modeling of the ARM summer 1997 IOP: Model formulation, results, uncertainties, and sensitivities. *J. Atmos. Sci.,* **60,** 607–625.

Khouider, B., and A. J. Majda, 2006: A simple multicloud parameterization for convectively coupled tropical waves. Part I: Linear analysis. *J. Atmos. Sci.,* **63,** 1308–1323.

Kiehl, J. T., J. J. Hack, G. B. Bonan, B. A. Boville, D. L. Williamson, and P. J. Rasch, 1998: The National Center for Atmospheric Research Community Climate Model: CCM3. *J. Climate,* **11,** 1131–1149.

Kiladis, G. N., K. H. Straub, and P. T. Haertel, 2005: Zonal and vertical structure of the Madden–Julian oscillation. *J. Atmos. Sci.,* **62,** 2790–2809.

Kuang, Z. M., 2008: A moisture–stratiform instability for convectively coupled waves. *J. Atmos. Sci.,* in press.

——, and C. S. Bretherton, 2004: Convective influence on the heat balance of the tropical tropopause layer: A cloud-resolving model study. *J. Atmos. Sci.,* **61,** 2919–2927.

——, and ——, 2006: A mass-flux scheme view of a high-resolution simulation of a transition from shallow to deep cumulus convection. *J. Atmos. Sci.,* **63,** 1895–1909.

——, P. N. Blossey, and C. S. Bretherton, 2005: A new approach for 3D cloud-resolving simulations of large-scale atmospheric circulation. *Geophys. Res. Lett.,* **32,** L02809, doi:10.1029/2004GL021024.

Lindzen, R. S., 1974: Wave-CISK in the Tropics. *J. Atmos. Sci.,* **31,** 156–179.

——, 2003: The interaction of waves and convection in the Tropics. *J. Atmos. Sci.,* **60,** 3009–3020.

Majda, A. J., and M. G. Shefter, 2001: Models for stratiform instability and convectively coupled waves. *J. Atmos. Sci.,* **58,** 1567–1584.

Mapes, B. E., 2000: Convective inhibition, subgrid-scale triggering energy, and stratiform instability in a toy tropical wave model. *J. Atmos. Sci.,* **57,** 1515–1535.

——, 2004: Sensitivities of cumulus-ensemble rainfall in a cloud-resolving model with parameterized large-scale dynamics. *J. Atmos. Sci.,* **61,** 2308–2317.

——, S. Tulich, J.-L. Lin, and P. Zuidema, 2006: The mesoscale

convection life cycle: Building block or prototype for large-scale tropical waves? *Dyn. Atmos. Oceans,* **42,** 3–29.

Neelin, J. D., I. M. Held, and K. H. Cook, 1987: Evaporation–wind feedback and low-frequency variability in the tropical atmosphere. *J. Atmos. Sci.,* **44,** 2341–2348.

Parsons, D. B., J.-L. Redelsperger, and K. Yoneyama, 2000: The evolution of the tropical western Pacific atmosphere-ocean system following the arrival of a dry intrusion. *Quart. J. Roy. Meteor. Soc.,* **126,** 517–548.

Raymond, D. J., and X. P. Zeng, 2005: Modelling tropical atmospheric convection in the context of the weak temperature gradient approximation. *Quart. J. Roy. Meteor. Soc.,* **131,** 1301–1320.

Redelsperger, J.-L., D. B. Parsons, and F. Guichard, 2002: Recovery processes and factors limiting cloud-top height following the arrival of a dry intrusion observed during TOGA COARE. *J. Atmos. Sci.,* **59,** 2438–2457.

Ridout, J. A., 2002: Sensitivity of tropical Pacific convection to dry layers at mid- to upper levels: Simulation and parameterization tests. *J. Atmos. Sci.,* **59,** 3362–3381.

Roca, R., J.-P. Lafore, C. Piriou, and J.-L. Redelsperger, 2005: Extratropical dry-air intrusions into the West African monsoon midtroposphere: An important factor for the convective activity over the Sahel. *J. Atmos. Sci.,* **62,** 390–407.

Sherwood, S. C., 1999: Convective precursors and predictability in the tropical western Pacific. *Mon. Wea. Rev.,* **127,** 2977–2991.

Sobel, A. H., and C. S. Bretherton, 2000: Modeling tropical precipitation in a single column. *J. Climate,* **13,** 4378–4392.

——, and ——, 2003: Large-scale waves interacting with deep convection in idealized mesoscale model simulations. *Tellus,* **55A,** 45–60.

——, S. E. Yuter, C. S. Bretherton, G. N. Kiladis, 2004: Large-scale meteorology and deep convection during TRMM KWAJEX. *Mon. Wea. Rev.,* **132,** 422–444.

Straub, K. H., and G. N. Kiladis, 2003: The observed structure of convectively coupled Kelvin waves: Comparison with simple models of coupled wave instability. *J. Atmos. Sci.,* **60,** 1655–1668.

Takayabu, Y. N., 1994: Large-scale cloud disturbances associated with equatorial waves. Part I. Spectral features of the cloud disturbances. *J. Meteor. Soc. Japan,* **72,** 433–449.

Takemi, T., O. Hirayama, and C. H. Liu, 2004: Factors responsible for the vertical development of tropical oceanic cumulus convection. *Geophys. Res. Lett.,* **31,** L11109, doi:10.1029/2004GL020225.

Tomita, H., H. Miura, S. Iga, T. Nasuno, and M. Satoh, 2005: A global cloud-resolving simulation: Preliminary results from an aqua planet experiment. *Geophys. Res. Lett.,* **32,** L08805, doi:10.1029/2005GL022459.

Tulich, S. N., D. A. Randall, and B. E. Mapes, 2007: Vertical-mode and cloud decomposition of large-scale convectively coupled gravity waves in a two-dimensional cloud-resolving model. *J. Atmos. Sci.,* **64,** 1210–1229

Wang, B., 1988: Dynamics of tropical low-frequency waves: An analysis of the moist Kelvin wave. *J. Atmos. Sci.,* **45,** 2051–2065.

Webster, P. J., and R. Lukas, 1992: TOGA COARE: The Coupled Ocean–Atmosphere Response Experiment. *Bull. Amer. Meteor. Soc.,* **73,** 1377–1416.

Wheeler, M., and G. N. Kiladis, 1999: Convectively coupled equatorial waves: Analysis of clouds and temperature in the wavenumber–frequency domain. *J. Atmos. Sci.,* **56,** 374–399.